Plant Communications
Research article

CellPress
Partner Journal

Complex genetic architecture underlying the plasticity of maize agronomic traits

Minliang Jin[1], Haijun Liu[2], Xiangguo Liu[3], Tingting Guo[1,4], Jia Guo[3], Yuejia Yin[3], Yan Ji[5], Zhenxian Li[6], Jinhong Zhang[6], Xiaqing Wang[1], Feng Qiao[1], Yingjie Xiao[1,4], Yanjun Zan[7,5,*] and Jianbing Yan[1,4,*]

[1]National Key Laboratory of Crop Genetic Improvement, Huazhong Agricultural University, Wuhan 430070, China

[2]Gregor Mendel Institute, Austrian Academy of Sciences, Vienna BioCenter, 1030 Vienna, Austria

[3]Institute of Agricultural Biotechnology, Jilin Academy of Agricultural Sciences, Changchun 130033, China

[4]Hubei Hongshan Laboratory, Wuhan 430070, China

[5]Key Laboratory of Tobacco Improvement and Biotechnology, Tobacco Research Institute, Chinese Academy of Agricultural Sciences, Qingdao 266000, China

[6]Institute of Agricultural Sciences of Xishuangbanna Prefecture of Yunnan Province, Jinghong 666100, China

[7]Umeå Plant Science Center, Department of Forestry Genetics and Plant Physiology, Swedish University of Agricultural Sciences, 90736 Umeå, Sweden

***Correspondence: Yanjun Zan (yanjun.zan@slu.se), Jianbing Yan (yjianbing@mail.hzau.edu.cn)**

https://doi.org/10.1016/j.xplc.2022.100473

ABSTRACT

Phenotypic plasticity is the ability of a given genotype to produce multiple phenotypes in response to changing environmental conditions. Understanding the genetic basis of phenotypic plasticity and establishing a predictive model is highly relevant to future agriculture under a changing climate. Here we report findings on the genetic basis of phenotypic plasticity for 23 complex traits using a diverse maize population planted at five sites with distinct environmental conditions. We found that latitude-related environmental factors were the main drivers of across-site variation in flowering time traits but not in plant architecture or yield traits. For the 23 traits, we detected 109 quantitative trait loci (QTLs), 29 for mean values, 66 for plasticity, and 14 for both parameters, and 80% of the QTLs interacted with latitude. The effects of several QTLs changed in magnitude or sign, driving variation in phenotypic plasticity. We experimentally validated one plastic gene, *ZmTPS14.1*, whose effect was likely mediated by the compensation effect of *ZmSPL6* from a downstream pathway. By integrating genetic diversity, environmental variation, and their interaction into a joint model, we could provide site-specific predictions with increased accuracy by as much as 9.9%, 2.2%, and 2.6% for days to tassel, plant height, and ear weight, respectively. This study revealed a complex genetic architecture involving multiple alleles, pleiotropy, and genotype-by-environment interaction that underlies variation in the mean and plasticity of maize complex traits. It provides novel insights into the dynamic genetic architecture of agronomic traits in response to changing environments, paving a practical way toward precision agriculture.

Key words: complex traits, phenotypic plasticity, QTL-by-environment interaction, crop improvement, *Zea mays*

Jin M., Liu H., Liu X., Guo T., Guo J., Yin Y., Ji Y., Li Z., Zhang J., Wang X., Qiao F., Xiao Y., Zan Y., and Yan J. (2023). Complex genetic architecture underlying the plasticity of maize agronomic traits. Plant Comm. **4**, 100473.

INTRODUCTION

Upon environmental change, plants display a plastic response, whereby a single genotype produces multiple phenotypes through changes in gene expression, physiology, and morphology (Sultan 2000; Nicotra et al., 2010). Population-level differences in plasticity will result in genotype-by-environment (G-by-E) interaction (Assmann 2013; El-Soda et al., 2014; Sasaki et al., 2015), releasing heritable variations (Pigliucci 2005; Schneider et al., 2011; Mangin et al., 2017; Vanous et al., 2019) that are highly relevant to complex trait variation and adaptation (Kang 1997; El-Soda et al., 2014; Gage et al., 2017; Kusmec et al., 2018). In the context of crop breeding, one strategy is to minimize plasticity to develop a cultivar with satisfactory performance across a wide range of environments (Lynch and Walsh 1998). Alternatively, performance can be maximized in individual

Published by the Plant Communications Shanghai Editorial Office in association with Cell Press, an imprint of Elsevier Inc., on behalf of CSPB and CEMPS, CAS.

environments by enriching environment-specific beneficial alleles that are conditional neutral or unfavorable in other environments (Jannink et al., 2010; Gage et al., 2017; Ge et al., 2022; Xiao et al., 2022). This is similar to how natural selection has acted on wild populations, in which local adaptation has resulted in genotypes with optimized phenotypes in their native environments that are often maladapted in new environments (Lazzaro et al., 2008; Hereford 2009; Anderson et al., 2013; Blanquart et al., 2013).

Increased plasticity may be the future of crop breeding and biodiversity management in light of climate change because such a strategy produces highly resilient genotypes for future challenges while achieving an optimal local phenotype. To achieve this goal, efforts have been made to study the genetic architecture of plasticity (Finlay and Wilkinson 1963; Gollob 1968; Jiang and Zeng 1995; Malosetti et al., 2013) and dissect the underlying QTLs (quantitative trait locus; El-Soda et al., 2014; Rauw and Gomez-Raya 2015; Kusmec et al. 2017, 2018; Li et al., 2019; Schneider et al., 2020). Studies in maize have revealed similarities and differences in the genetic architecture of trait mean and plasticity (Kusmec et al., 2017; Li et al., 2019), suggesting that breeders could manipulate trait mean and plasticity semi-independently to meet the challenge of feeding the growing population. Other investigations have demonstrated the role of plastic QTLs in heterosis and adaptation from the tropical to the temperate zone, paving the way for genomics-enabled crop improvement by manipulating phenotypic plasticity (Li et al., 2018; Liu et al., 2021).

Despite the insights gained through these efforts, several questions remain. First, there is a lack of understanding of the dynamics of complex trait genetic architectures across environments, such as the effects of specific environmental factors on range-wide complex trait variation. How dynamic are the genetic architectures of agronomic traits over a major production zone? Which alleles are favored at each production site? Do they have genetic effects on multiple traits with antagonistic pleiotropy? How much genetic gain can be achieved by exploiting these alleles? Second, in Fisher's decomposition of phenotype mean (Fisher, 1918), the environmental effect is a combinatory effect of multiple environmental factors such as temperature, day length, and soil conditions. With an increased ability to quantify air and soil conditions using developments in remote sensing, it is of great interest to deconstruct combinatory environmental effects into effects from concrete environmental factors and study their effects on complex trait variation and prediction. Finally, plasticity is often treated as a composite index (Finlay and Wilkinson 1963; Gollob 1968; Jiang and Zeng 1995; Malosetti et al., 2013), neglecting the fact that plasticity is environmentally dependent, being variable when quantified using different combinations of environments. With a growing number of possible environments to investigate, it is worthwhile to differentiate plasticity quantified using an overall index and refine plasticity measures from specific combinations of environments.

To provide deeper insight into these questions, we developed the complete-diallel plus unbalanced breeding-derived inter-cross (CUBIC) population of 1404 advanced inter-cross lines from 24 representative breeding founders (Liu et al., 2020a) and studied the variation in 23 key agronomic traits at five sites spanning China's major summer maize production zone (Figure 1A) from the northeast at Jilin (JL; N43°42′, E125°18′) to the central plains at Henan (HN; N35°27′, E114°01′). We revealed major contributions from latitude-related environmental factors to across-site phenotypic variation in flowering time traits but not in other traits. We dissected the within- and across-environment variation into 109 QTLs with complex genetic architectures involving multiple alleles, pleiotropy, and G-by-E interaction. In particular, we found that extensive QTL-by-environment interactions and dynamics in mean QTL effects across environments were driving the variation in phenotypic plasticity. A joint model with site-specific predictions and higher accuracy was developed by integrating genetic diversity, environmental variation, and their interaction, paving the way for genomics-directed maize improvement.

RESULTS

The effect of clinal variation in environmental factors on the mean and plasticity of 23 complex maize traits

We surveyed the performance of 23 traits across five sites from N43°42′ (JL) to N35°27′ (HN; Figure 1A), spanning the major Chinese summer maize production zone. Nearly all traits were significantly correlated with latitude, suggesting a general contribution of latitudinally variable environmental factors to maize agronomic trait variation (Figure 1B–1F and Supplemental Figure 1; Supplemental Tables 1 and 2). Flowering time traits (days to tassel [DTT], days to silking [DTS], and days to anthesis [DTA]) displayed the strongest latitudinal variation, and the trait median measured at the northernmost site (JL) was ∼1.5 times larger than that at the southernmost site (HN) (Supplemental Figure 1; Supplemental Table 2). By contrast, clinal variation in plant architecture traits (plant height [PH], ear height, and ear leaf width [ELW]) and yield traits was weaker, being more distinctive between the northern (JL, Liaoning [LN], and Beijing [BJ]) and southern (Hebei Province and HN) sites (Figure 1B and 1C and Supplemental Figure 1).

All 23 traits displayed variation in phenotypic plasticity (Figure 1G), and yield traits were more plastic than flowering time and plant architecture traits. Contributions from environment and G-by-E interaction varied significantly among the three categories of traits. For example, G-by-E made a greater contribution to proportion of variance explained (median = 32.8%; Figure 1I) for the across-site variation in yield traits, consistent with the observation that the proportions of non-additive variance for yield traits were also higher than those for flowering and architecture traits (Figure 1H). These results illustrated a general contribution from environmental factors and their interaction with genotype to variation in mean and plasticity of maize complex traits; the contribution from G-by-E was more prominent for yield traits, indicating the importance and potential value of studying plasticity for yield improvement.

Dynamic and complex genetic architecture underlying the mean and plasticity of maize agronomic traits

For each of the 23 traits, we derived two types of measures to quantify phenotypic plasticity. Type I included 10 measures (Ungerer et al., 2003; Zan and Carlborg 2020a) calculated as pairwise differences among five sites to capture specific plasticity (SP), and type II included 4 measures representing overall plasticity (OP): the coefficient of variation from raw (CV)

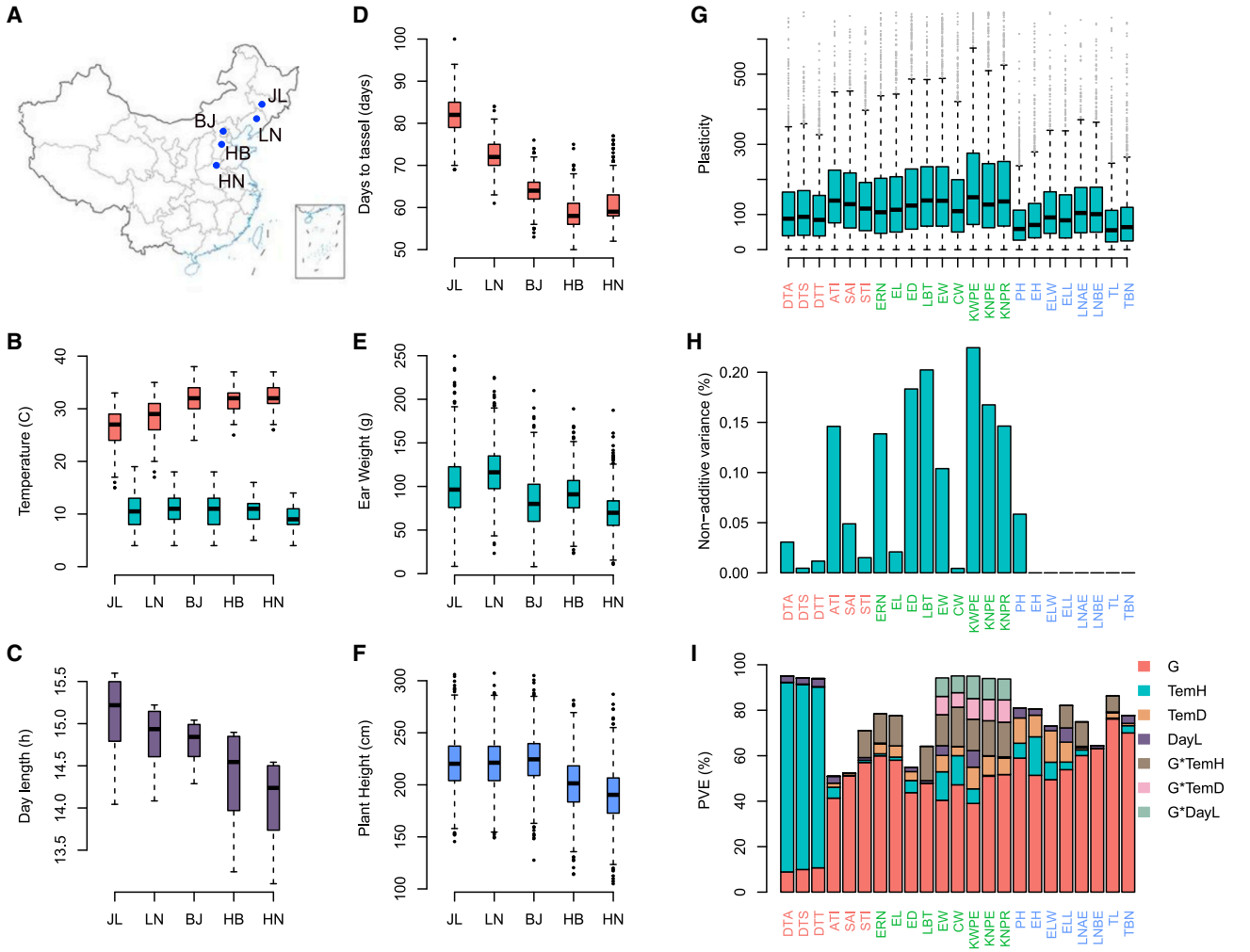

Figure 1. Environmental variations across China's major summer maize production zone and their effects on across-site variation of maize complex traits.(A) The five surveyed sites spanning China's major maize production zone, where 23 agronomic traits were phenotyped for 1404 inbred lines.

(B) Boxplot illustrating the highest daily temperature (TemH; red) and daily temperature difference (TemD; cyan) from sowing to flowering at the five sites.

(C) Boxplot of day length (DayL; purple) from sowing to flowering at the five sites.

(D–F) Boxplot of days to tassel (DTT; red) **(D)**, ear weight (EW; cyan) **(E),** and plant height (PH; blue) **(F)** measured at the five sites.

(G) Boxplot of phenotypic plasticity measured as the CV of the rank across sites (Methods). The 23 traits (labeled on the x axis) were grouped into three categories: flowering traits highlighted in red; plant architecture traits labeled in green; and yield traits labeled in blue.

(H) Bar plot of the proportion of non-additive variance (differences between broad-sense heritability, capturing the additive and non-additive effect, and narrow-sense heritability, capturing only the additive effect). Each vertical bar represents a trait, and the height of the bar is proportional to the difference between corresponding broad- and narrow-sense heritability.

(I) Contributions of genotype, three environmental factors (TemH, TemD, and DayL), and their interactions to the across-site variation of the 23 agronomic traits. Each vertical bar represents a trait, with the corresponding trait name labeled on the x axis. The colored segments within each bar represent the contributions from genotype, TemD, TemH, DayL, and their interactions with genotype, as indicated in the legend. The height of the segment is proportional to the percentage of variance explained (PVE) by the corresponding variance component.

(Zan and Carlborg 2020a) and rank-transformed data (VarR) (Zan and Carlborg 2020a), the second principal component (PC2) (Zan and Carlborg 2020a), and Finlay–Wilkinson regression (FWR) (Lian and de Los Campos 2015) (Supplemental Figure 2; Methods). Together with the trait mean value from five sites (mean) and BLUP (best linear unbiased prediction), these four types of measures (SP, OP, mean, and BLUP) were used to scan for QTLs underlying trait mean and plasticity using genome-wide association analysis (Methods). In the following section, we first illustrate results from DTT as an example and then expand to results from all 23 traits. Hereafter, the 4 types of measures are referred to as DTT_{BLUP}, DTT_x (mean measured at site x), SP-$DTT_{x\text{-}y}$ (SP measured as DTT_x–DTT_y (where x and y are the site names), and OP-DTT_z (OP calculated using method z; z is described under Methods).

Loci associated with variation in mean and plasticity measures for DTT: Dynamic QTL effects across environments lead to variation in plasticity

A total of 15 QTLs were identified: 11 QTLs for SP/OP-DTT, 7 QTLs for DTT_{mean}/DTT_{BLUP}, and 3 overlapping QTLs

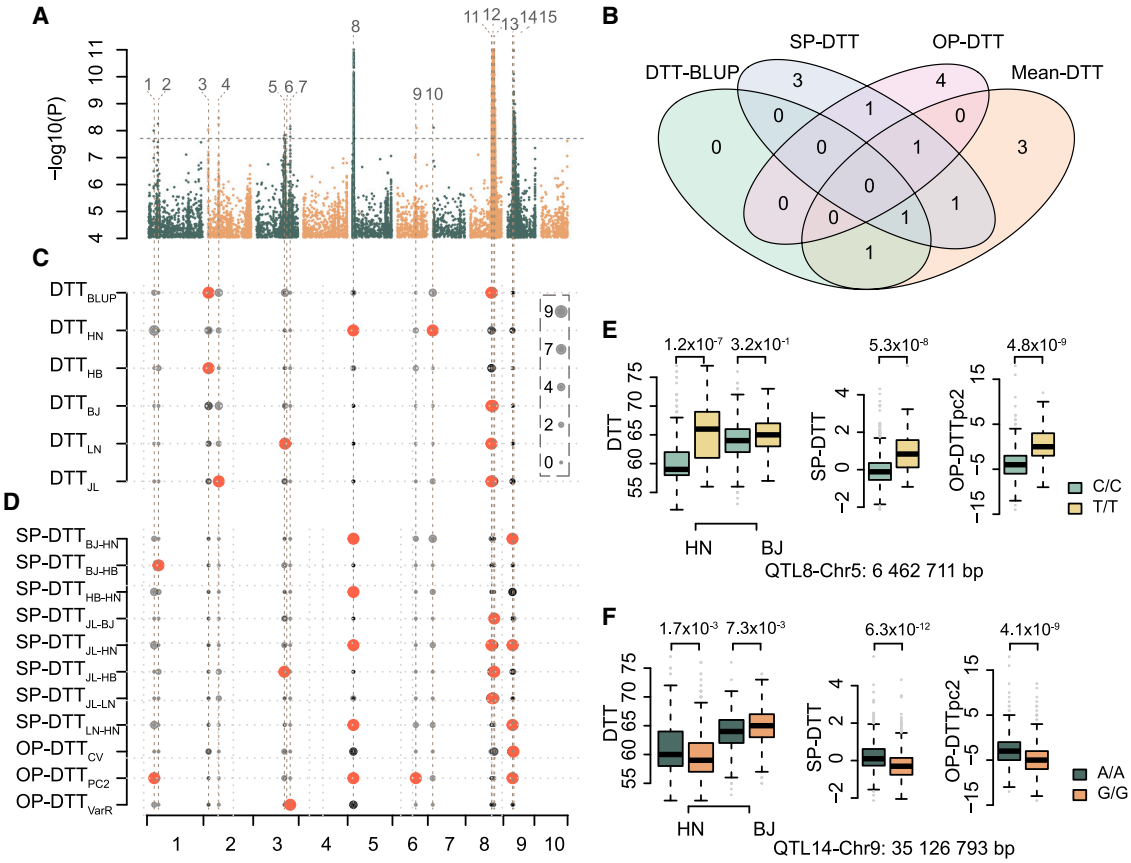

Figure 2. Summary of the QTLs associated with mean and plasticity measures for DTT.

(A) Manhattan plots overlaying GWAS results for the 20 mean and plasticity measurements for DTT. The black horizontal dashed line indicates the Bonferroni-corrected genome-wide significance threshold derived as 0.05/Me (Me is the effective number of independent markers; Methods), and the vertical dashed black lines indicate the positions of detected QTLs, labeled from 1–15.

(B) Venn diagram illustrating the overlap among QTLs detected for the 4 types of DTT measurements.

(C) QTLs associated with the DTT means measured at five sites and the DTT_{BLUP} (y axis). Each dot represents a SNP, and the size of the dot is proportional to its −Log10 *p* value, as indicated in the legend on the right. Loci with a *p* value above the genome-wide significance threshold are colored in red.

(D) QTLs associated with the DTT plasticity measurements (labeled on the y axis). Two SP measurements with no significant QTLs have been omitted.

(E and F) Genotype-to-phenotype maps, highlighting the increased power to detect additional loci by analyzing plasticity measurements, for DTT_{HN}, DTT_{BJ}, DTT_{HN-BJ}, and DTT_{pc2} at two QTLs, one on chromosome 5 (6 462 711 bp) and a second on chromosome 9 (35 126 793 bp).

(Figure 2A–2D; Supplemental Tables 3–5). The majority of the QTLs were detected for DTT_{mean} and SP/OP-DTT, whereas only 2 QTLs were detected for DTT_{BLUP} (Figure 2B). By contrasting the genetic effects of QTLs across sites, two types of QTLs, whose effects changed in magnitude or sign, were associated with DTT plasticity. For example, QTL8 (Figure 2A–2C and 2E) showed a significant effect on DTT_{HN} ($P = 1.2 \times 10^{-7}$; Figure 2D) and the SP measure DTT_{HN-BJ} ($P = 5.3 \times 10^{-8}$; Figure 2E) but had no effect on the other DTT mean and plasticity measurements (Figure 2C–2E), indicating that changes in the magnitude of genetic effects contributed to the variation in DTT plasticity. By contrast, QTL14 (Figure 2A–2C and 2F) was exclusively detected for several DTT plasticity measurements but not for any DTT_{mean} or DTT_{BLUP} measurements. However, the genetic effects of QTL14 on DTT_{mean} changed direction from positive (DTT_{HN}, 0.6 ± 0.2 days; $P = 1.7 \times 10^{-3}$; Figure 2F) to negative (DTT_{BJ}, −0.5 ± 0.2 days; $P = 7.3 \times 10^{-3}$; Figure 2F), leading to a significant association with SP DTT_{HN-BJ} (1.1 ± 0.2 days; $P = 6.3 \times 10^{-12}$; Figure 2D) and OP DTT_{pc2} ($P = 4.1 \times 10^{-9}$). These results indicated that changes in magnitude and/or signs of genetic effects across sites caused variation in plasticity, which could be detected by genome-wide association studies (GWASs) of SP and OP measurements. The changing genetic effects highlighted the effect of QTL-by-environment interaction on variation in mean and plasticity of complex traits.

Loci associated with variation in the remaining traits: A complex genetic architecture involving multiple alleles, pleiotropy, and G-by-E interaction underlies variation in maize complex traits

For the 23 traits, we identified 109 QTLs for the 4 types of mean and plasticity measurements (Figure 3A; Supplemental Figure 3; Supplemental Tables 3, 4, and 6). The QTLs overlapped partially, and 1.8%, 34.9%, 19.3%, and 21.1% of the QTLs were unique to BLUP, SP, OP, and mean measurements, respectively (Figure 3B). As illustrated in the previous section, QTLs associated with SP measurements likely changed the sign or magnitude of their genetic effects (Figure 2E and 2F) across sites. This was supported by testing the interaction between the detected QTLs and the five sites: 80.0% of the QTLs showed significant interactions with latitude (Supplemental

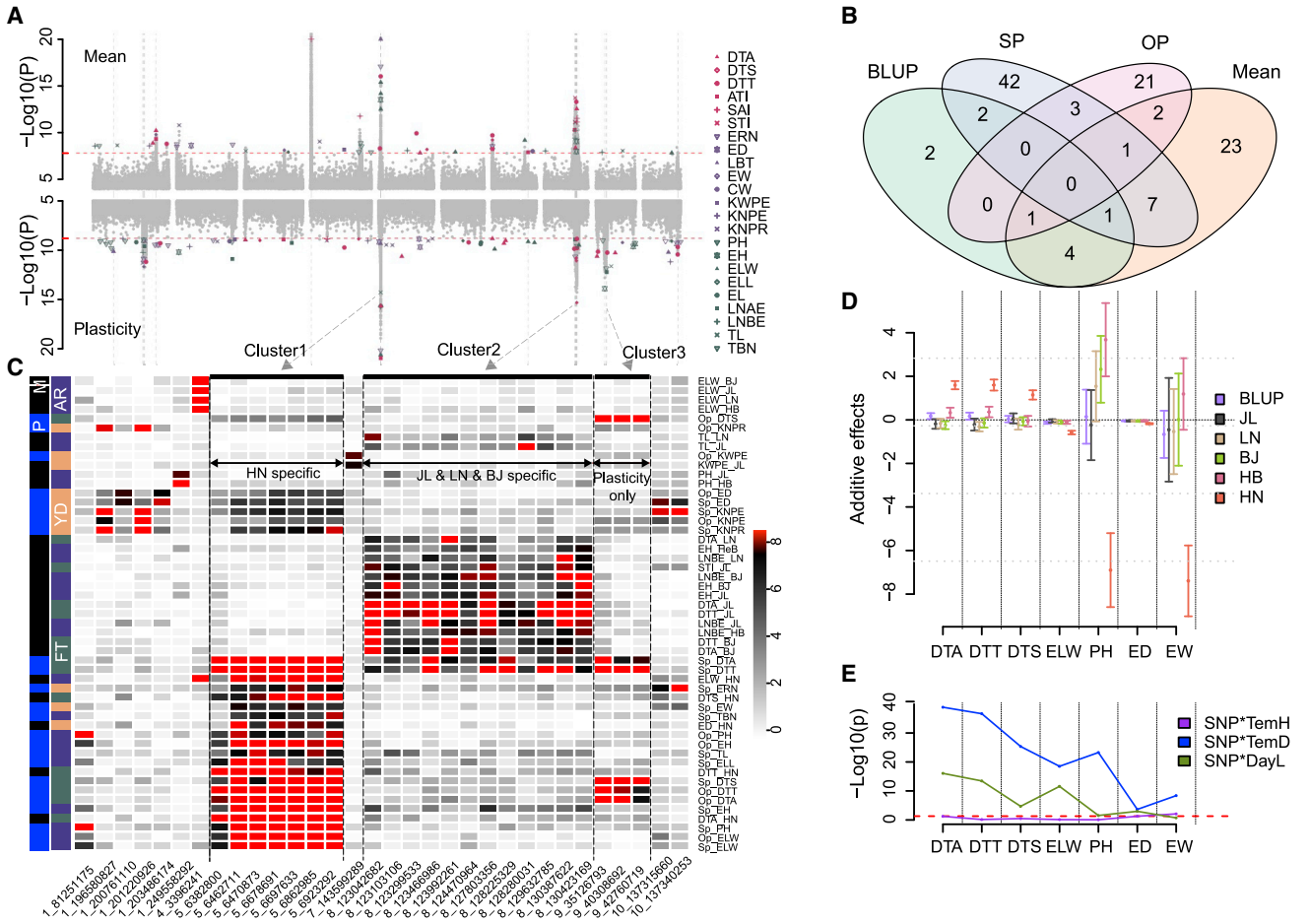

Figure 3. Association results of mean and plasticity for all 23 traits.

(A) Manhattan plots of GWASs from all scans, with the top panel for means and bottom panel for plasticity measurements. The red horizontal dashed lines indicate the Bonferroni-corrected genome-wide significance threshold. The vertical dashed gray lines highlight the sites of 32 SNPs associated with more than two measurements.

(B) Venn diagram illustrating the overlap among QTLs detected for the four types of measurements.

(C) A heatmap illustrating the *p* values of the 32 SNPs detected for more than two measurements (here, SNPs were used instead of QTLs because one QTL sometimes includes multiple SNPs that are physically close to each other but not in high LD). Each cell represents the −Log10 (*p* value) of a particular SNP (x axis) associated with a specific trait (y axis on the right). The outer index on the left side marks the mean (M; black) or plasticity (P; blue) of the traits. The inner index marks the corresponding trait types: plant architecture (AR; purple), flowering time (FT; olive green), and yield (YD; orange). For each trait, only the lowest *p* values are indicated for specific P (SP) or overall P (OP), labeled as SP trait or OP trait.

(D) The additive effects varied across sites, exemplified by cluster 1 (chromosome 5: 6 462 711 bp) on multiple traits. The traits are separated by dashed vertical lines and labeled on the x axis. For each trait, the measurements for BLUP and individual sites are ordered (from left to right) as indicated in the color legend. Medians and standard errors are shown by the middle point and error bars, respectively.

(E) The *p* values associated with tests of the interaction between this SNP (chromosome 5: 6 462 711 bp) and the three environmental factors.

Table 7; Methods). These results demonstrated the dynamic genetic effects of mean QTLs across sites and highlighted partial overlap between QTLs regulating mean and plasticity, as reported in previous studies (Kusmec et al., 2017; Li et al., 2019; Liu et al., 2021).

One cluster, spanning 540 kb on chromosome 5, involved 7 SNPs that were physically close together but not in high linkage disequilibrium (LD; cluster 1 in Figure 3A and 3C, QTL 8 in Figure 2A); it was detected for multiple trait means and plasticity measures at HN. A detailed exploration showed that multiple haplotypes were underlying this region; each of the 7 SNPs tagged a unique haplotype (Supplemental Figure 4), suggesting that the 24 founders carried different functional variants. Each of the 7 SNPs was simultaneously associated with multiple trait means at HN, including DTT_{HN}, DTA_{HN}, ELW_{HN}, ear weight $(EW)_{HN}$, PH_{HN}, and multiple SP measurements (Figure 3C and 3D), indicating that this region was highly pleiotropic. The genetic effect of this QTL was unique to HN for all associated traits; the "TT" genotype increased DTT, DTA, and DTS, and the "CC" genotype decreased ED (ear diameter), EW, ELW, and PH at HN but not at other sites, likely because of interaction with temperature (especially daily temperature difference [TemD]) and day length (DayL) (Figure 3E and Supplemental Figure 5), providing an ideal candidate for use in targeted breeding at HN.

A second cluster, spanning 7.4 Mb on chromosome 8, showed allelic heterogeneity and pleiotropic effects on multiple flowering

and plant architecture traits (cluster 2 in Figure 3A and 3C and Supplemental Figure 6). However, the genetic effects were unique to the three northern sites (JL, LN, and BJ; Figure 3C). Compared with cluster 1, whose effects were unique to HN, such regional effects on multiple northern sites may have led to the detection of this QTL for multiple sites and BLUP measurements.

A third cluster (cluster 3 in Figure 3A and 3C) contributed exclusively to variation in plasticity measurements for all flowering time traits (DTT, DTA, and DTS) owing to the change of additive effects from negative to positive (Figure 2F).

These results illustrate a complex genetic architecture involving multiple alleles, pleiotropy, and G-by-E interaction underlying variation in maize complex traits. Detection of QTLs unique to HN and the three northern sites demonstrates a variable genetic architecture for maize complex traits across sites, possibly because of clinal variation in QTL effects.

Fine-mapping the detected QTLs

A few QTL peaks, such as the QTLs on chromosome 5 (6–7 Mb; Figure 3A and Supplemental Figure 4) and chromosome 8 (123–130 Mb; Figure 3A and Supplemental Figure 6) were simultaneously associated with multiple trait means and plasticity measurements, possibly as a consequence of extended LD. Fine-mapping the causal variants underlying each mean and plasticity QTL and determining whether these signals are tagging a common signal that is simultaneously associated with multiple trait means and plasticity measures or whether they are multiple variants, each associated with one measure but in tight LD with each other, is a daunting task. Although detailed analysis (Supplemental note) showed that a large proportion of the SNPs were tagging the same causal variants (Supplemental Figures 4 and 6), there seemed to be multiple association signals (Id SNPs, defined here as signals that have significant *p* values when fitted together in a linear model but do not necessarily have zero LD) underlying the same QTL (Supplemental Figures 4 and 6) for several mean or plasticity measures. For example, a detailed exploration of the chromosome 5 QTL showed that multiple Id SNPs were tagging different combinations of functional haplotypes (Supplemental Figure 4), illustrating a complex genetic architecture involving allelic heterogeneity, multiple alleles, pleiotropy, and G-by-E interaction at the same time. To pinpoint the causal genes in the presence of such complexity, we used a gene-based test (Law et al., 2015) aggregating summary statistics on SNPs up- and downstream of the annotated protein-coding genes. We detected 300 genes (Supplemental Table 8), 24% of which were simultaneously associated with both mean and plasticity measurements (106 for mean, 122 for plasticity, 72 for both). Among these genes, the maize FT gene *ZCN8* was detected in both mean and plasticity scans of flowering traits, whereas *ZCN18* was only associated with STI (silk-tassel interval) plasticity (Meng et al., 2011). A benzoxazinone synthesis gene cluster including *bx1/2/3/8* on chromosome 4 was associated with the mean of ELW. Similar conditional effects have also been found in mutants and plants overexpressing multiple flowering genes in *Arabidopsis*, such as *PRR3* in the circadian clock (Murakami et al., 2004), *PIF4* in the ambient temperature pathway (Kumar et al., 2012), and *HXK1* in the sugar pathway (Matsoukas et al., 2013; Liu et al., 2022). Although future experiments are required to determine the biological mechanism underlying such variation, the validation of two candidate genes in our study suggests that the effect of genes on complex traits may, in general, be context dependent.

The possible molecular basis of phenotypic plasticity

Previously, we linked *ZmTPS14.1*, which was located in the QTL on chromosome 8 (cluster 2 in Figure 3), to variation in flowering time mean (Liu et al., 2020b). Here, this QTL was simultaneously associated with mean and plasticity variation in multiple traits at the genome-wide ($P = 1.53 \times 10^{-8}$) or suggestive significance threshold ($P = 1.00 \times 10^{-5}$). The tagging SNPs showed interactions with all 3 environmental factors, suggesting a general contribution of QTL-by-environmental-factor interaction to variation in phenotypic plasticity.

To experimentally validate and evaluate the plasticity effects of *ZmTPS14.1*, we planted knockout lines of *ZmTPS14.1* obtained in a previous study (Liu et al., 2020b) in JL (north China, N43°30′, E124°49′) and Hainan (HaiN, south China, N18°34′, E108°43′) and compared the measured flowering time phenotypes. Consistent with the association results, the female flowering time (DTS) of knockout lines was earlier in HaiN but not significantly different in JL compared with that of wild-type lines (Figure 4A and Supplemental Figures 7A and 8A; Supplemental Table 9). To explore the underlying molecular basis, we analyzed an in-house time-course transcriptome dataset generated from reference accession B73 under long-day and short-day conditions (Figure 4B). The expression of *ZmTPS14.1* under both day-length conditions changed in the same direction along the time course (Figure 4B), suggesting that there was no day-length-dependent expression response for *ZmTPS14.1*.

Because it has been proposed that plastic response may involve developmental switch genes (Sommer 2020), we explored whether plastic effects of genes at the center of the regulatory pathway were mediated by or interacted with downstream genes. We therefore evaluated the expression of candidates downstream of *ZmTPS14.1*. *ZmTPS14.1* encodes trehalose-6-phosphate synthase (TPS), which converts glucose-6-phosphate into trehalose-6-phosphate, regulating vegetative development and flowering by the miR156/SPL pathway (Tsai and Gazzarrini 2014). The expression pattern of *ZmSPL6,* an SPL (Squamosa Promoter-binding protein-Like) family member downstream of *ZmTPS14.1*, differed significantly in response to DayL (Figure 4B). Knockout lines of *ZmSPL6* showed earlier female flowering in JL but no significant change in HaiN compared with wild-type lines, which was also observed in association analysis (Figure 4A and Supplemental Figures 7B and 8B; Supplemental Table 9), suggesting that temperature and DayL were important factors for the plastic effect of *ZmSPL6*. Thus, we proposed a compensation mechanism from *ZmSPL6* to *ZmTPS14.1* in DTS plasticity (Figure 4C). Under long-day conditions, the continuous increase in expression of *ZmSPL6* could make up for the knockout of *ZmTPS14.1*, resulting in no phenotypic difference between the *ZmTPS14.1* knockout lines and the wild type (Figure 4A). No such compensation occurred under short-day conditions; thus, we observed a phenotypic difference between *ZmTPS14.1* knockout and wild-type lines under short-day conditions (Figure 4A and 4C). This compensation mechanism

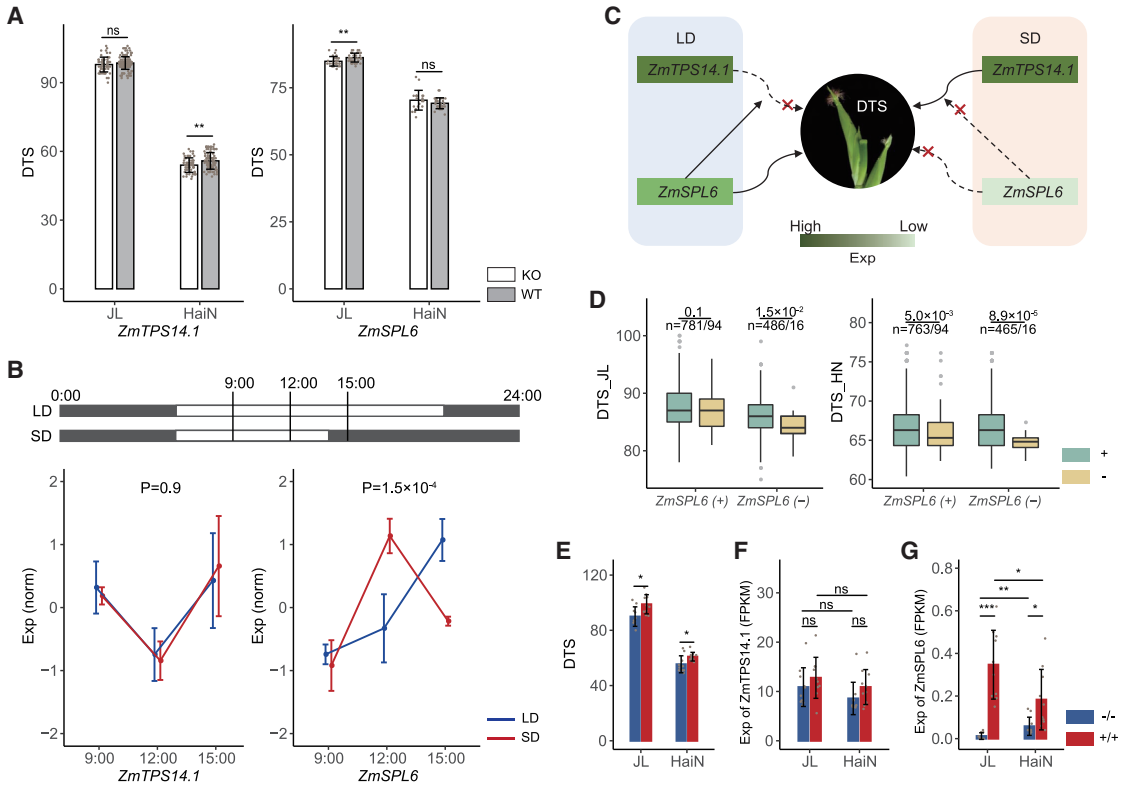

Figure 4. The interaction between *ZmTPS14.1* and *ZmSPL6* reveals the genetic basis of phenotypic plasticity in flowering time.

(A) Phenotypes (days to silking [DTS]) of knockout lines and wild types of *ZmTPS14.1* and *ZmSPL6* at two field plantations; one plantation at JL represents Jilin (N43°30′, E124°49′) and the other at HaiN represents Hainan (N18°34′, E108°43′). Error bars represent standard deviations. $^{**}p < 0.01$ (Student's *t*-test). ns, not significant.

(B) Sampling diagram of the time-course experiment in B73 under long-day (LD) and short-day (SD) conditions. The gray and white areas represent the dark and light time periods. Leaf tissues were harvested at three time points (9:00, 3 h of light; 12:00, 6 h of light; 15:00, 9 h of light/1 h of dark). The expression patterns of *ZmTPS14.1* and *ZmSPL6* at three time points under LD conditions (blue) and SD conditions (red) are shown. The y axis represents gene expression, which was obtained from standardization of raw read counts followed by *Z* score normalization. Error bars represent standard errors.

(C) The proposed compensation interaction model between *ZmSPL6* and *ZmTPS14.1*. *ZmSPL6* is highly expressed under LD conditions, which could affect female flowering, but its expression is suppressed under SD conditions, showing no effect on flowering. The *ZmTPS14.1* knockout lines showed a difference in flowering time under SD conditions but not LD conditions because of the compensation effect of *ZmSPL6*. Solid lines indicate the presence of regulation, and dashed lines indicate the absence of regulation.

(D) Phenotype (DTS in JL and HN) comparison between two alleles of *ZmTPS14.1* (chromosome 8: 123 138 468 bp; C/C genotype → +; T/T genotype → −) in different allelic backgrounds of *ZmSPL6* under LD (JL) and SD (HN) conditions (chromosome 3: 159 420 596 bp; G/G genotype → +; T/T genotype → −). The *p* values were obtained by Student's *t*-test.

(E) Phenotypes (DTS) of lines with *ZmTPS14.1* (+)/*ZmSPL6* (+) (+/+, n = 10) and *ZmTPS14.1* (−)/*ZmSPL6* (−) (−/−, n = 10) at two field plantations; one plantation at JL represents Jilin (N43°30′, E124°49′), and the other at HaiN represents Hainan (N18°34′, E108°43′). Error bars represent standard deviations.

(F) The expression of *ZmTPS14.1* in lines with +/+ and −/− at two field plantations.

(G) The expression of *ZmSPL6* in lines with +/+ and −/− at two field plantations.

$^{*}p < 0.05$, $^{**}p < 0.01$, $^{***}p < 0.001$ (Student's *t*-test).

was also reflected in the CUBIC population (Figure 4D). Under long-day conditions (JL), *ZmTPS14.1* showed a significant association ($P = 1.5 \times 10^{-2}$) with DTS in the TT allele background of *ZmSPL6* (−) but no significant association in the GG allele background of *ZmSPL6* (+). Under short-day conditions (HN), a significant association between *ZmTPS14.1* and DTS was detected in both the *ZmSPL6* (−) ($P = 8.9 \times 10^{-5}$) and *ZmSPL6* (+) ($P = 5.0 \times 10^{-3}$) backgrounds (Figure 4D). This compensation mechanism was validated in a maize association panel (Li et al., 2012a) whose flowering time and RNA sequencing data were available for JL and HaiN (unpublished data). Consistent with findings from the CUBIC population, the *ZmTPS14.1* (−)/*ZmSPL6* (−) lines (referred to as −/−, n = 10) flowered earlier than the *ZmTPS14.1* (+)/*ZmSPL6* (+) lines (+/+, n = 10) under both long-day (JL, $P = 1.1 \times 10^{-2}$) and short-day (HaiN, $P = 2.5 \times 10^{-2}$; Figure 4E) conditions, and there was no significant difference in *ZmTPS14.1* expression between −/− and +/+ lines or long-day and short-day conditions. By contrast, *ZmSPL6* expression was significantly higher in +/+ lines under both long-day ($P = 9.9 \times 10^{-5}$) and short-day conditions ($P = 2.2 \times 10^{-2}$; Figure 4F). In the +/+ genetic background, *ZmSPL6* showed higher expression under long-day than short-day conditions ($P = 2.7 \times 10^{-2}$; Figure 4G). The opposite pattern was observed in −/− lines: *ZmSPL6* expression was higher under short-day than long-day

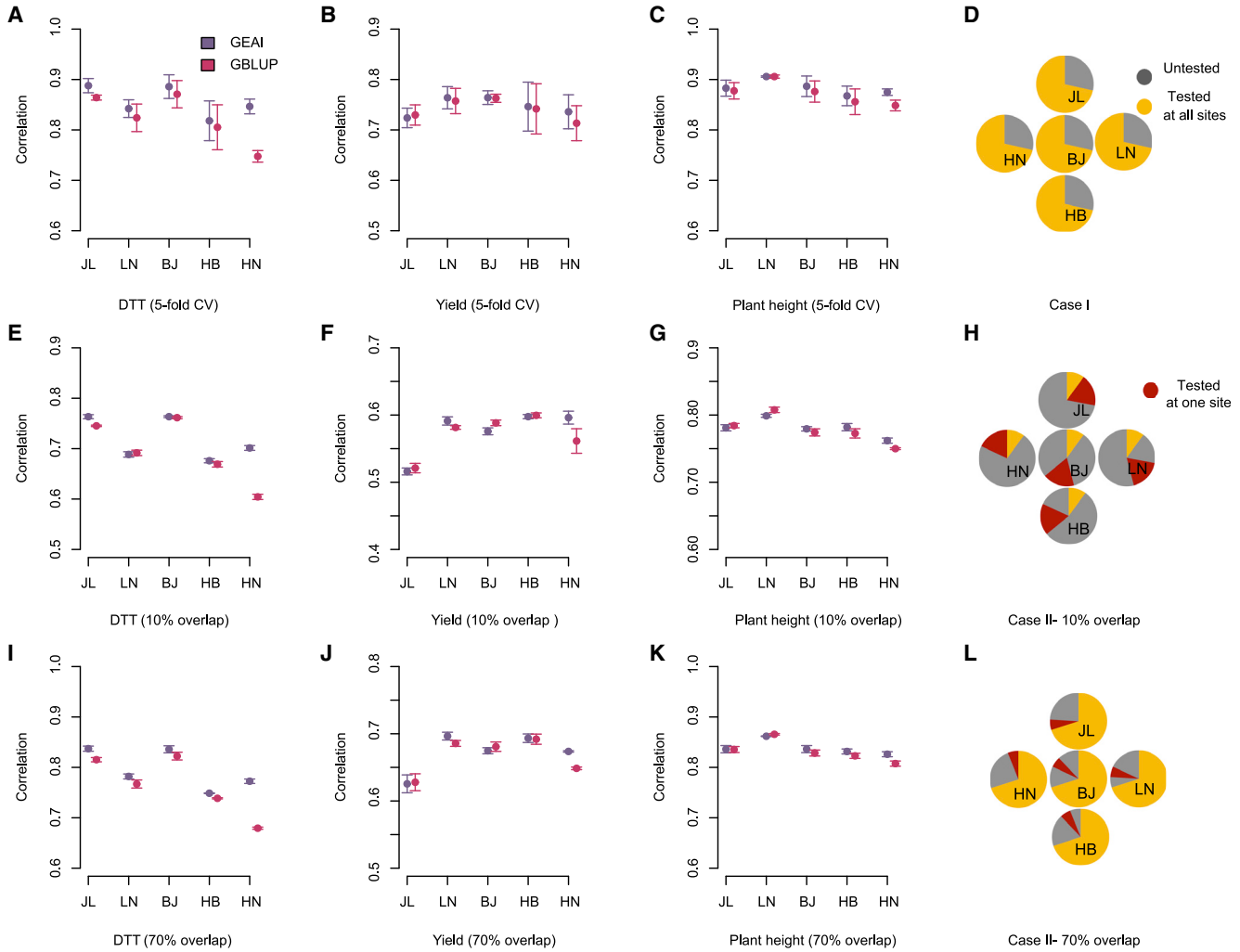

Figure 5. Performance of the GEAI model for site-specific complex trait prediction.

(A–C) Predictability of untested lines at any of the five sites using all lines phenotyped across the five sites as training data for **(A)** DTT, **(B)** EW, and **(C)** PH.

(E–G) Prediction accuracy for untested lines at any of the five sites for **(E)** DTT, **(F)** EW, and **(G)** PH when 10% of the lines were phenotyped at all five sites and the remaining lines were divided into five even sets, with each set phenotyped at only one of the five sites.

(I–K) Prediction accuracy for **(I)** DTT, **(J)** EW, and **(K)** PH when 70% of the lines were phenotyped at all five sites and the remaining lines were divided into five even sets, with each set phenotyped at only one of the five sites.

(D, **H**, and **L)** Schematics of the prediction design for case I **(D)** and case II (**H** and **L**).

conditions ($P = 8.1 \times 10^{-3}$; Figure 4G), although its expression was lower compared with the +/+ genetic background. The plastic gene *ZmTPS14.1* was thus validated, and its effect was likely mediated by the compensation effect of *ZmSPL6* from the downstream pathway, which may be dependent on the genetic background.

Accounting for dynamics in genetic architecture improved complex trait prediction across environments

We evaluated the potential of integrating genetic diversity, environmental variation, and their interaction in complex trait prediction by jointly modeling genotype, environment, and their interaction (referred to as the GEAI model; Methods). Two cross-validation schemes were considered. First, we explored the ability to predict untested lines (newly developed lines) at the five sites using 5-fold cross-validation. In this scenario, 80% of the lines with phenotypes measured at all five sites were randomly selected as a training set, and the remaining 20% of lines, whose phenotypes were masked as NA, were used as a test set (Figure 5J). Within-site Pearson correlation (r) between predicted and measured phenotypes was used to evaluate the accuracy of the predicted phenotype at each of the five sites. Compared with the GBLUP, with a universal prediction for all sites, our model not only provided site-specific predictions but also increased prediction accuracy for the majority of traits and sites (83.0% of all traits and sites; Supplemental Table 10; Methods). The averaged prediction accuracy for DTT, PH, and EW increased by 3.4%, 0.6%, and 1.1%, respectively, and the increase in prediction accuracy was more pronounced at HN (increased by 9.9%, 2.2%, and 2.6% for DTT, PH, and EW, respectively; Figure 5A–5C).

In the second case, we explored a series of more challenging designs in which only a core set of lines (10%–70%) was phenotyped at all five sites, with the aim of predicting the performance

of unphenotyped lines at each site (incomplete field trial). This was motivated by the fact that a fraction of the breeding material is routinely evaluated in different years and sites, resulting in sparse phenotype records in a long-term breeding program. In this scenario, we randomly sampled 10%–70% of the lines to mimic a core set of lines with measured phenotypes at all five sites. The remaining lines were divided evenly into five sets whose phenotypes were masked at four of the five sites (Figure 5H and 5L). The aim was to evaluate whether the GEAI model could outperform GBLUP in terms of within-site Pearson correlation. The GEAI model showed higher accuracy for almost all traits and sites. For example, at 10% overlap, our GEAI model outperformed GBLUP predictions ($P = 4.0 \times 10^{-3}$) by 2.4% on average and increased prediction accuracy at four of the five sites by 0.4%–9.7% for DTT. At 70% overlap, the increase in accuracy at each site was greater than at 10% overlap (1.0%–10.3%; Figure 5E–5G and 5I–5K), and the average accuracy was increased to 3.4%. As the number of lines phenotyped at all sites increased from 10% to 70%, the average accuracy and site-specific accuracy increased (Supplemental Figure 9). Our study thus highlighted the potential of integrating QTL-by-environment interaction for understanding and predicting complex traits.

DISCUSSION

By surveying the performance of a genetically diverse population across China's major summer maize production zone, we were able to quantify contributions from specific environmental factors to the variation in 23 complex traits, detect plastic QTLs, and provide a more accurate site-specific complex trait prediction model.

Contribution of environmental factors to variation in the mean and plasticity of maize complex traits

We quantified phenotypic plasticity as a response to differences between particular environmental sites and across all five sites, resulting in multiple plasticity measures for the same genotype. Despite a high overall correlation among these plasticity measurements, different QTLs were detected, indicating that these measures captured different aspects of plasticity with complementary information. Such differences in quantifying phenotypic plasticity may be highly relevant to applications in which the test site and target site are clearly defined. In particular, when the mechanism by which environmental factors interact with a plastic QTL is known, the performances of large germplasm collections could be accurately predicted in various deployment environments, facilitating precise breeding designs in the future.

Among the 23 traits, yield traits were more plastic than other traits and involved larger contributions from temperature and DayL as well as a larger proportion of G-by-E interactions. A similar result was reported by D'Andrea et al., (2013). A possible explanation could be that yield traits are the result of combined effects from vegetative and reproductive growth, with demonstrated contributions from temperature and photoperiod (Yoshida 1981; Wallace et al., 1993) that are likely to be equally important. Reliable partition of the variance across five sites to particular environmental factors is challenging because they are highly correlated with latitude. Additional studies are needed to explore the effects of specific environmental factors on variation in trait mean and plasticity and to determine how differences in genetic architecture among traits cause such differences in phenotypic plasticity.

The genetic architectures underlying trait mean and plasticity

Consistent with previous studies (Prado et al., 2014; Li et al., 2019), we found partial overlaps between QTLs associated with trait mean and plasticity. However, our interpretation is that, conceptually, when treating phenotypic plasticity as a measure of change for one polygenic trait across environments, such overlap is expected. We also expect that (1) plasticity is polygenic as a result of the polygenic architecture for the trait itself in different environments, (2) the degree of overlap between QTLs underlying trait mean and plasticity may vary across studies because of detection power, and (3) QTLs whose genetic effects differ among environments are more likely to affect the variability of plasticity. Taking DTT as an example, we detected 7 loci for DTT mean and 9 loci for DTT plasticity, four of which overlapped. Changes in the magnitude or sign of QTL effects resulted in variability in DTT plasticity, providing support for the allelic sensitivity model (Des Marais et al., 2013). Even though we did not detect the chromosome 9 QTL in the DTT mean scan at a genome-wide significance level, a moderate association was found at a lower significance threshold. In line with this result, when we aggregated the allelic effects of mean or plasticity QTLs that were not detected at a genome-wide significance level, we found that they contributed significantly to variation in mean and plasticity measurements as a group (Supplemental Figure 10; Supplemental Table 11). We also found that SNPs with larger variability in effect size across environments were more likely to be detected in a mean scan and less likely to be picked up in a BLUP scan (Supplemental Figure 11), indicating that greater variability in effect size across environments could undermine the detection power of a BLUP scan. Given the polygenic and dynamic genetic architecture of trait means across environments reported here and in previous research (Zan and Carlborg 2020a, 2020b), there may be a tighter connection between the genetic regulation of trait mean and plasticity than has previously been acknowledged.

Complex trait prediction across environments

When a small proportion of plant material overlapped (10%) among sites, we found a number of sites in which GBLUP outperformed GEAI (Figure 5 and Supplemental Figure 8). This is because estimation of QTL-by-environment effects is strongly biased when the number of observations is low. Despite the low number of overlapping materials, on an average level, the GEAI model always offered higher prediction accuracy, and the value of the GEAI model increased as the proportion of overlapping plant material increased. When 100% of the plant material overlapped among environments, prediction accuracy increased by 0.6%–3.7% on average, and GEAI outperformed GBLUP in 83% of cases (Figure 5). It is likely that the linear model over- or underpredicts effects in extreme cases; i.e., overestimating or underestimating effects at HN or JL, leaving a few cases where GBLUP outperforms GEAI. Although it is not perfect, we recommend using GEAI whenever a

large proportion of materials overlap among sites in order to achieve a higher overall performance before improved nonlinear models are available. Compared with previously developed reaction norm models (Heslot et al., 2014; Jarquín et al., 2014; Jarquin et al., 2020) for across-environment prediction, the strength of the GEAI model is that it includes interactions between detectable QTLs and environmental conditions. The downside is that interactions between polygenic background and environmental conditions are missed, and information from correlated traits is not fully exploited. Future developments in integrating the reaction norm model and GEAI model and attempts to borrow information from more environmental variables (Guo et al., 2020) and correlated traits would further improve prediction accuracy.

METHODS

Experimental design

We developed a CUBIC population of 1404 inbred maize lines and surveyed their performance for 23 agronomic traits at five sites in China's major maize production zone, with longitudinal variation from E114°01′ at HN to E125°18′ at JL and latitudinal variation from N43°42′ at HN to N35°27′ at HN. A detailed description of the development of this population is available in Liu et al. (2020a). In brief, the inbred lines were derived from 24 elites representing 4 divergent heterotic groups using cycles of random mating, selection, and inbreeding (Liu et al., 2020a). In 2014, all lines were planted at five sites, including JL (N43°42′, E125°18′), LN (N42°03′, E123°33′), BJ (N40°10′, E116°21′), Hebei province (N38°39′, E115°51′), and HN (N35°27′, E114°01′), with a random order in each environment to eliminate potential confounding effects. About 17 individual plants were planted for each line, and one fixed line (Chang7-2) was planted after every 50th line to evaluate field spatial heterogeneity. Because the phenotypes of this check line showed very limited variation across the field, no further phenotypic corrections were performed on the other lines; thus, the raw measurements were analyzed directly. Twenty-three agronomic traits, including 6 phenology traits, 8 plant architecture traits, and 9 yield traits, were phenotypically evaluated. Except for six flowering traits that were scored as the median values of replicated lines, all traits were scored as the means of replicates (Supplemental Table 12). Three environmental variables, including daily highest temperature (TemH), TemD, and DayL, were obtained by first extracting the site-specific daily variables from the corresponding closest weather station at http://data.sheshiyuanyi.com (available in Supplemental Table 13). These daily variables from sowing to flowering at each site were averaged to obtain one value representing the environmental records at each site. All 1404 lines were re-sequenced, and the called genotypes are available for download in Liu et al. (2020a). The raw fastq files were uploaded to the NCBI Sequence Read Archive with ID PRJNA597703, and the called SNP data in PLINK format are available at https://pan.baidu.com/s/1AsPJLTe–gU5EN8aFTMYPA. In total, 4.38 M SNPs with MAF (minor allele frequency) > 0.03 and LD $\leq$ 0.9 in a 100-kb sliding window were retained for downstream analysis.

Partitioning the phenotypic variance into contributions from genotype, environmental factors, and their interactions

The phenotypic variance was partitioned into contributions from genotype, G-by-E, and residual (environment) by fitting the following model:

$$\bar{y}_{ij} = u + id_i + TemH_j + TemD_j + DayL_j + id_i * TemH_j + id_i * TemD_j + id_i * DayL_j + e_{ij} \quad \text{(Equation 1)}$$

This model was fitted for each of the 23 traits one at a time. $\bar{y}_{ij}$ is the trait mean/median of individual i (i = 1…n, n = 1404, number of individuals) at site j (j = 1…q; q = 5, number of sites); id_i is the line id (genotype) coded as a factor; and $TemH_j$, $TemD_j$, and $DayL_j$ are three environmental variables representing TemH, TemD, and DayL at site j. These environmental factors were coded as numeric, assuming a linear relationship with the phenotypic measurements. id_i * $TemH_j$, id_i * $TemD_j$, and id_i * $DayL_j$ are the interaction terms (G-by-E) between a particular line (genotype) and the corresponding environmental factors (environment). The relative contributions to total phenotypic variance from genotype and G-by-E were estimated by their respective sum of squares (the sum of squares for id is calculated as $\sum_1^p (id_i - \overline{id})^2$, and the sum of squares for the interaction terms id $*E$ are calculated as $\sum_1^n (id_i * E_j - \overline{id_i * E_j})^2$), where E stands for TemH, TemD, or DayL.

Trait BLUP was estimated using the following model:

$$\bar{y}_{ij} = u + Z\mu + e_{ij} \quad \text{(Equation 2)}$$

$\bar{y}_{ij}$ and e_{ij} are the same as model 1. μ is a vector of random effects, representing the BLUP values of 1404 individuals; Z is the design matrix connecting the BLUPs with the corresponding phenotypic measurements; and μ is a vector of length 1404 that follows N (0, $I\,\sigma_g^2$).

Estimating broad/narrow-sense heritability, non-additive variance, and genetic correlations

Broad-sense heritability was estimated by ANOVA based on a simple linear model fitting phenotype measured at five sites as the response variable, with sites coded as a factor and line id as an explanatory variable.

$$\bar{y}_{ij} = u + id_i + e_{ij} \quad \text{(Equation 3)}$$

Variance explained by line id divide the phenotypic variance was treated as estimates for broad-sense heritability.

A linear model (4) was used to estimate the narrow-sense heritability for BLUP values of all 23 traits.

$$\bar{y} = u + Z\mu + e \quad \text{(Equation 4)}$$

Here, $\bar{y}$ is a vector of the 1404 trait means/medians for each individual (genotype) at each tested site. e is the normally distributed residual, u is the population mean, and μ is a random effect vector of the breeding values for the 1404 individuals. Z is the corresponding design matrix obtained from a Cholesky decomposition of the kinship matrix G, estimated using the genome-wide markers with GCTA (Yang et al., 2011). The Z matrix satisfies ZZ' = G; therefore, $\mu \sim$is normally distributed N (0, $I\,\sigma_g^2$). e is the residual variance with e $\sim$ N (0, $I\sigma_e^2$). The narrow-sense heritability of the fitted phenotype was calculated as the intraclass correlation $h^2 = \sigma_g^2/(\sigma_g^2 + \sigma_e^2)$. AI-REML implemented in GCTA was used to obtain these estimates (Yang et al., 2011). The additive genetic variance was σ_g^2. Non-additive variance was estimated as the difference between broad-sense heritability and narrow-sense heritability (trait BLUP).

Similarly, a bivariant mixed model was fitted to obtain estimates of the genetic correlation between measurements obtained from two individual sites. Ten models were thus fitted to obtain all pairwise genetic correlations among five sites. $\overline{Y}$, μ, and u from model (4) were updated to an n × 2 matrix, with n being the number of individuals and each column vector representing measurements obtained from a particular site. This model was fitted using the "reml-bivar" module (Li et al., 2012b) implemented in GCTA software (Yang et al., 2011); details of this model are available in Lee et al., (2012).

Quantification of phenotypic plasticity for the 23 agronomic traits

Because all 1404 maize lines were phenotyped for 23 agronomic traits across five sites, we quantified and studied the genetics of maize complex

trait plasticity in response to longitudinal and latitudinal environmental variation. The phenotypic plasticity was classified into two categories (Supplemental Figure 2B–2E). The first category is OP, describing plasticity across all studied environments, and the second category, SP, is more unique to certain pairs of sites and only captures the plasticity across two environments. The motivation underlying such classification is that some individuals are robust across all but a few studied sites, whereas other individuals are plastic across most sites.

One metric, the pairwise difference in phenotypic value between two sites, was used to quantify SP (Supplemental Figure 2A). Using DTT measured at JL and HN as an example, the differences in measured DTT values for all individuals (SP_{DTT}^{JL-HN} = DTT_{JL} -DTT_{HN}) describe the SP between HN and JL (Supplemental Figure 2B; Ungerer et al., 2003). Although $DTT_{JL} - DTT_{HN}$ and $DTT_{HN} - DTT_{JL}$ differ in sign, we chose only one of them because the sign difference does not affect the GWAS power. The only difference is the interpretation of the estimated effect size, which should be interpreted together with the direction of the subtraction. Four additional approaches were used to quantify OP (Supplemental Figure 2C–2E). First, principal-component analysis was used to quantify OP. The influence of phenotype measurements at individual sites on the PCs can be captured in the loadings (Yano et al., 2019; Supplemental Figure 2C). Because PC2 captures more variation in OP (PC2 is more representative of the phenotype differences among environments because the loading differs more on the second PC), we used PC2 as a measure of overall phenotypic plasticity. Second, the across-environment variance (VAR) of the rank-transformed phenotype proposed in Vanous et al. (2019) was used (Supplemental Figure 2D), and the CV (Vanous et al., 2019) was also used to account for the mean difference. The fourth score for OP uses FWR (Weber and Scheiner 1992; Lian and de Los Campos 2015) to partition the phenotype into two components; one is constant across environments, and the other responds dynamically to environmental changes. Using a linear mixed model, the phenotype of each line is partitioned into these two components, and the plasticity component is used as a measurement of plasticity. Together, the described approaches resulted in 14 measurements of phenotypic plasticity (abbreviated as SP, PCA, VarR, CV, and FWR). These three metrics yield 14 plasticity measurements for each trait.

GWAS for trait mean/median and plasticity measurements

To detect genetic polymorphisms underlying variation in agronomic trait mean and plasticity, we fitted the following linear mixed model:

$$Y = \mu + X\beta + Zu + e \quad \text{(Equation 5)}$$

where Y, μ, Z, u, and e are the same as those defined in model (4). X is a matrix containing the genotypes of the tested SNP (coded as 0/2 for minor/major-allele homozygous genotypes, respectively). β is a vector including the estimated additive allele-substitution effect for the tested SNP. First, a genome-wide analysis across all genotyped SNPs was conducted using GEMMA (Zhou and Stephens 2012). A subsequent conditional analysis was performed, in which all top associated SNPs (SNPs with the highest p value from each association QTL in the initial genome-wide analysis scan) were included as covariates in the design matrix X to screen for additional association signals. The conditional analysis was repeated until no more SNPs were above the significance threshold, and it was implemented in the "cojo" module of GCTA (Yang et al., 2012). The LD was high in this population, making a Bonferroni correction assuming that all tested markers were statistically independent too conservative. Therefore, we estimated the effective number of independent markers (Me) (Li et al., 2012b) and derived a less conservative genome-wide significance threshold of 0.05/Me (1.53×10^{-8} equivalent to $-\text{Log}_{10}$ p value = 7.81).

A colocalization test separates linkage from pleiotropy at regions where multiple signals are associated with multiple traits

Multiple association signals, each associated with one or multiple traits, were colocalized at the same genomic regions. Because the level of LD between the lead SNPs was very low, we could not directly determine whether multiple independent signals detected in multiple scans and physically close to each other derived from (1) one association signal simultaneously associated with multiple scans (pleiotropy) or (2) multiple associations, each associated with one scan but in tight LD with each other. To distinguish these possibilities, we performed a multi-trait colocalization analysis (Supplemental note). This method estimates a posterior probability of whether multiple traits share a common causal variant using summary statistics from each trait (Berisa and Pickrell 2016; Foley et al., 2021). We first binned the genome into 1-Mb bins. Scans with Id SNPs that fell into consecutive bins were aggregated and tested for colocalization using the "hyprcoloc" R package (Berisa and Pickrell 2016; Foley et al., 2021). Given the complex population history (multi-parental) and a limited number of recombinations, some of the associated SNPs were very close to each other but not in high LD. To make a comparison among the 4 types of measurements, we arbitrarily grouped SNPs within less than 1 Mb into a single QTL.

Gene-based test to prioritize candidate genes

The LD was too extensive to directly pinpoint genes underlying the associated loci. We therefore used a set-based analysis that aggregates summary statistics from all variants 50 kb up/downstream of the tested gene to obtain one p value to represent its significance. The summary association statistics, including effect sizes, standard errors, minor allele frequencies, and sample size, were first extracted from the GEMMA association output and then entered into the "fastBAT" module in GCTA (Bakshi et al., 2016); 39 155 genes annotated in the B73 reference genome version 3 were used to bin the summary statistics to perform the set analysis (Law et al., 2015).

Testing for G-by-E interaction of detected QTLs

We tested the interaction between QTLs associated with each of the 23 traits in at least one of the five sites, one QTL and one trait at a time, by fitting the model below:

$$\bar{y}_{ij} = u + id_i + site_j + QTL_i + e_{ij} \quad \text{(Equation 6)}$$

$$\bar{y}_{ij} = u + id_i + site_j + QTL_i + QTL_i * site_j + e_{ij} \quad \text{(Equation 7)}$$

This model was fitted for each of the 23 traits one at a time. $\bar{y}_{ij}$ is the trait mean/median of individual i (i = 1…n, n = 1404, number of individuals) at site j (j = 1…q; q = 5, number of sites), id_i is the line id (genotype) coded as a factor, and $site_j$ is a vector of characters representing the site where the measurements were made. QTL_i is the genotype of id_i at the tested QTL, and $QTL_i * site_j$ is the interaction terms (G-by-E) between a particular QTL and the sites (environments). A likelihood ratio test comparing the models with (model 6) and without (model 7) the interaction between sites was performed to calculate p values. The significance threshold was calculated as 0.05 divided by the number of tests ($0.05/143 = 3.49 \times 10^{-04}$).

Experimental validation of maize flowering genes

Knockout lines of *ZmTPS14.1* and *ZmSPL6* were generated using a high-throughput genome-editing system (Liu et al., 2020b). In brief, line-specific sgRNAs (small guide RNA) were filtered based on the assembled pseudo-genome of the receptor KN5585. The double sgRNA pool approach was used to construct vectors. The vectors were transformed into the receptor KN5585. The genotype of gene-edited lines was identified by PCR amplification and Sanger sequencing using target-specific primers (Supplemental Table 14). The phenotypes of knockout lines and the wild type were

investigated in JL (Gongzhuling, JL province, N43°30′, E124°49′) and HaiN (Sanya, HaiN province, N18°34′, E108°43′).

Time-course transcriptome

B73 seeds were planted under two conditions: long-day conditions (14 h light and 10 h dark) and short-day conditions (8 h light and 16 h dark). Leaf tissues were harvested at 3 time points during one day at stage vegetative 4 (four fully extended leaves). RNA from eighteen samples (2 conditions × 3 time points × 3 replicates) was sequenced on the HiSeq 3000 platform. Low-quality reads were removed with Trimmomatic (Bolger et al., 2014). STAR (Dobin et al., 2013) was used to align the RNA sequencing reads to the reference genome. HTSeq (Anders et al., 2015) was used to obtain gene-level counts from the resulting BAM files, and genes with significant expression changes were detected with ImpulseDE2 (Fischer et al., 2018).

Estimating the contribution from mean and plasticity QTLs to the variation in mean and plasticity measurements

We quantified the contribution of mean and plasticity QTLs to variation in trait mean and plasticity by fitting the following model:

$$Y = X_1\beta_1 + X_2\beta_2 + Zu + e \quad \text{(Equation 8)}$$

Here, Y is a vector of length n (n = 1404), representing the trait mean or plasticity measurement. The joint contributions from mean and plasticity QTLs were modeled in $X_1\beta_1$ and $X_2\beta_2$, where X_1 and X_2 are the design matrices and β_1 and β_2 are the corresponding effect sizes. Z, u, and e are the same as defined in model 5. The Z matrix satisfies ZZ' = G, and u is therefore normally distributed ($u \sim N(0, I\,\sigma_g^2)$). Contributions from mean and plasticity QTLs were then calculated with $Var_m = \frac{Var(X_1\beta_1)}{Var(y)}$ and $Var_p = \frac{Var(X_2\beta_2)}{Var(y)}$.

Predicting the site-specific performance of the 23 traits

We fitted the following models to predict the performance of each site for the 23 traits one at a time:

$$Y = X_1\beta_1 + Zu + e \quad \text{(Equation 9)}$$

$$Y = X_2\beta_2 + Zu + e \quad \text{(Equation 10)}$$

Here, Y is a vector of length n*p (n = 1404, number of individuals; p = 5, number of sites; n*p = 7020) representing the trait means measured at five sites; u is a vector of length n*p representing the breeding value of the n maize line; and e is the randomly distributed residual with length n*p. The Z matrix satisfies ZZ' = G ⊗ *I*, where G is the identity by state matrix, and *I* is a diagonal matrix of pxp. X_1 is a design matrix with one column of 1 representing column mean and an additional 4 columns representing the environmental effects from the remaining 4 sites, and β_1 is a vector of corresponding effect sizes. X_2 includes all columns from X_1 and additional columns with genotypes of the k QTLs associated with the mean and plasticity measures of the tested trait and additional columns representing the interaction between the k QTLs and the five sites, capturing the effects of QTL-by-environmental-factor interaction. The fitted values from model 9 are referred to as GBLUP predictions, whereas the fitted values from model 10 are referred to as GEAI predictions. These models were fitted using the "rrBLUP" (Endelman 2011) package in R (https://www.R-project.org/). In the first case, 80% of the lines with phenotypes measured from all five sites were used as a training set, and the remaining 20% of lines, whose phenotypes were masked as NA (not available), were used as a test set. Within-site r^2 between predicted and measured phenotypes was used to evaluate the accuracy of a predicted phenotype at each of the five sites. In the second case, we randomly sampled 10%–70% of the lines as a core set of lines that have measured phenotypes at all five sites, and the remaining lines were divided evenly into five sets whose phenotypes were masked randomly at four of the five sites. All lines with measured phenotypes were used as a training set, and lines masked as NA were used as a test set. Accuracy was estimated as the regression r^2 between measured and predicted phenotypes within each site.

SUPPLEMENTAL INFORMATION

Supplemental information is available at *Plant Communications Online*.

FUNDING

This research was funded by the Natural Science Foundation of China (31961133002, 31901553, and 31771879); the National Key Research and Development Program of China (2020YFE0202300); the Science and Technology Major Program of Hubei Province (2021ABA011), the Swedish Research Council for Environment, Agricultural Sciences, and Spatial Planning (2019-01600); the Key Science and Technology Project of the China National Tobacco Corporation (110202101040 JY-17), and the Jilin Scientific and Technological Development Program (20190201290JC).

AUTHOR CONTRIBUTIONS

J.Y. and Y.Z. designed and supervised this study. H.L., X.W., F.Q., and Y.X. collected raw data. Y.Z., M.J., and H.L. performed the data analysis. M.J., X.L., J.G., Y.Y., Y.J., Z.L., and J.Z. conducted the experiments. Y.Z., M.J., and J.Y. wrote the manuscript.

ACKNOWLEDGMENTS

We thank the Swedish National Infrastructure for Computing (SNIC) for support with computational resources through the High Performance Computing Centre North (HPC2N, SNIC 2020/9-117) and the Uppsala Multidisciplinary Centre for Advanced Computational Science (UPPMAX). We also thank the bioinformatics computing platform of the National Key Laboratory of Crop Genetic Improvement, Huazhong Agricultural University, for computational support. No conflict of interest is declared.

Received: June 14, 2022
Revised: August 21, 2022
Accepted: November 7, 2022
Published: January 14, 2023

REFERENCES

Anders, S., Pyl, P.T., and Huber, W. (2015). HTSeq–a Python framework to work with high-throughput sequencing data. Bioinformatics **31**:166–169.

Anderson, J.T., Lee, C.-R., Rushworth, C.A., Colautti, R.I., and Mitchell-Olds, T. (2013). Genetic trade-offs and conditional neutrality contribute to local adaptation. Mol. Ecol. **22**:699–708.

Assmann, S.M. (2013). Natural variation in abiotic stress and climate change responses in Arabidopsis: implications for Twenty-first-century agriculture. Int. J Plant Sci. **174**:3–26.

Bakshi, A., Zhu, Z., Vinkhuyzen, A.A.E., Hill, W.D., McRae, A.F., Visscher, P.M., and Yang, J. (2016). Fast set-based association analysis using summary data from GWAS identifies novel gene loci for human complex traits. Sci. Rep. **6**:32894.

Berisa, T., and Pickrell, J.K. (2016). Approximately independent linkage disequilibrium blocks in human populations. Bioinformatics **32**:283–285.

Blanquart, F., Kaltz, O., Nuismer, S.L., and Gandon, S. (2013). A practical guide to measuring local adaptation. Ecol. Lett. **16**:1195–1205.

Bolger, A.M., Lohse, M., and Usadel, B. (2014). Trimmomatic: a flexible trimmer for Illumina sequence data. Bioinformatics **30**:2114–2120.

D'Andrea, K.E., Otegui, M.E., Cirilo, A.G., and Eyhérabide, G.H. (2013). Parent–progeny relationships between maize inbreds and hybrids: analysis of grain yield and its determinants for contrasting soil nitrogen conditions. Crop Sci. **53**:2147–2161.

Des Marais, D.L., Hernandez, K.M., and Juenger, T.E. (2013). Genotype-by-environment interaction and plasticity: exploring genomic responses of plants to the abiotic environment. Annu. Rev. Ecol. Evol. Syst. **44**:5–29.

Dobin, A., Davis, C.A., Schlesinger, F., Drenkow, J., Zaleski, C., Jha, S., Batut, P., Chaisson, M., and Gingeras, T.R. (2013). STAR: ultrafast universal RNA-seq aligner. Bioinformatics **29**:15–21.

El-Soda, M., Malosetti, M., Zwaan, B.J., Koornneef, M., and Aarts, M.G.M. (2014). Genotype × environment interaction QTL mapping in plants: lessons from Arabidopsis. Trends Plant Sci. **19**:390–398.

Endelman, J.B. (2011). Ridge regression and other kernels for genomic selection with R package rrBLUP. Plant Genome **4**:250–255.

Finlay, K., and Wilkinson, G. (1963). The analysis of adaptation in a plant-breeding programme. Aust. J. Agric. Res. **14**:742–754.

Fischer, D.S., Theis, F.J., and Yosef, N. (2018). Impulse model-based differential expression analysis of time course sequencing data. Nucleic Acids Res. **46**:e119.

Fisher, R.A. (1918). The correlation between relatives on the supposition of mendelian inheritance. Trans. R Soc. Edin. **53**:399–433.

Foley, C.N., Staley, J.R., Breen, P.G., Sun, B.B., Kirk, P.D.W., Burgess, S., and Howson, J.M.M. (2021). A fast and efficient colocalization algorithm for identifying shared genetic risk factors across multiple traits. Nat. Commun. **12**:764.

Gage, J.L., Jarquin, D., Romay, C., Lorenz, A., Buckler, E.S., Kaeppler, S., Alkhalifah, N., Bohn, M., Campbell, D.A., Edwards, J., et al. (2017). The effect of artificial selection on phenotypic plasticity in maize. Nat. Commun. **8**:1348.

Ge, J., Wang, J., Pang, H., Li, F., Lou, D., Fan, W., Liu, Z., Li, J., Li, D., Nong, B., et al. (2022). Genome-wide selection and introgression of Chinese rice varieties during breeding. *J. Genet. Genomics* **49**:492–501.

Gollob, H.F. (1968). A statistical model which combines features of factor analytic and analysis of variance techniques. Psychometrika **33**:73–115.

Guo, T., Mu, Q., Wang, J., Vanous, A.E., Onogi, A., Iwata, H., Li, X., and Yu, J. (2020). Dynamic effects of interacting genes underlying rice flowering-time phenotypic plasticity and global adaptation. Genome Res. **30**:673–683.

Hereford, J. (2009). A quantitative survey of local adaptation and fitness trade-offs. Am. Nat. **173**:579–588.

Heslot, N., Akdemir, D., Sorrells, M.E., and Jannink, J.L. (2014). Integrating environmental covariates and crop modeling into the genomic selection framework to predict genotype by environment interactions. Theor. Appl. Genet. **127**:463–480.

Jannink, J.-L., Lorenz, A.J., and Iwata, H. (2010). Genomic selection in plant breeding: from theory to practice. Brief. Funct. Genomics **9**:166–177.

Jarquín, D., Crossa, J., Lacaze, X., Du Cheyron, P., Daucourt, J., Lorgeou, J., Piraux, F., Guerreiro, L., Pérez, P., Calus, M., et al. (2014). A reaction norm model for genomic selection using high-dimensional genomic and environmental data. Theor. Appl. Genet. **127**:595–607.

Jarquin, D., Howard, R., Crossa, J., Beyene, Y., Gowda, M., Martini, J.W.R., Covarrubias Pazaran, G., Burgueño, J., Pacheco, A., Grondona, M., et al. (2020). Genomic prediction enhanced sparse testing for multi-environment trials. G3 **10**:2725–2739.

Jiang, C., and Zeng, Z.B. (1995). Multiple trait analysis of genetic mapping for quantitative trait loci. Genetics **140**:1111–1127.

Kang, M.S. (1997). Using genotype-by-environment interaction for crop cultivar development. Adv. Agron. **62**:199–252.

Kumar, S.V., Lucyshyn, D., Jaeger, K.E., Alós, E., Alvey, E., Harberd, N.P., and Wigge, P.A. (2012). Transcription factor PIF4 controls the thermosensory activation of flowering. Nature **484**:242–245.

Kusmec, A., de Leon, N., and Schnable, P.S. (2018). Harnessing phenotypic plasticity to improve maize yields. Front. Plant Sci. **9**:1377.

Kusmec, A., Srinivasan, S., Nettleton, D., and Schnable, P.S. (2017). Distinct genetic architectures for phenotype means and plasticities in Zea mays. Nat. Plants **3**:715–723.

Law, M., Childs, K.L., Campbell, M.S., Stein, J.C., Olson, A.J., Holt, C., Panchy, N., Lei, J., Jiao, D., Andorf, C.M., et al. (2015). Automated update, revision, and quality control of the maize genome annotations using MAKER-P improves the B73 RefGen_v3 gene models and identifies new genes. Plant Physiol. **167**:25–39.

Lazzaro, B.P., Flores, H.A., Lorigan, J.G., and Yourth, C.P. (2008). Genotype-by-environment interactions and adaptation to local temperature affect immunity and fecundity in Drosophila melanogaster. PLoS Pathog. **4**:e1000025.

Lee, S.H., Yang, J., Goddard, M.E., Visscher, P.M., and Wray, N.R. (2012). Estimation of pleiotropy between complex diseases using single-nucleotide polymorphism-derived genomic relationships and restricted maximum likelihood. Bioinformatics **28**:2540–2542.

Li, C., Wu, X., Li, Y., Shi, Y., Song, Y., Zhang, D., Li, Y., and Wang, T. (2019). Genetic architecture of phenotypic means and plasticities of kernel size and weight in maize. Theor. Appl. Genet. **132**:3309–3320.

Li, H., Peng, Z., Yang, X., Wang, W., Fu, J., Wang, J., Han, Y., Chai, Y., Guo, T., Yang, N., et al. (2012a). Genome-wide association study dissects the genetic architecture of oil biosynthesis in maize kernels. Nat. Genet. **45**:43–50.

Li, M.-X., Yeung, J.M.Y., Cherny, S.S., and Sham, P.C. (2012b). Evaluating the effective numbers of independent tests and significant p-value thresholds in commercial genotyping arrays and public imputation reference datasets. Hum. Genet. **131**:747–756.

Li, X., Guo, T., Mu, Q., Li, X., and Yu, J. (2018). Genomic and environmental determinants and their interplay underlying phenotypic plasticity. Proc. Natl. Acad. Sci. USA **115**:6679–6684.

Lian, L., and de Los Campos, G. (2015). FW: an R package for Finlay-Wilkinson regression that incorporates genomic/pedigree information and covariance structures between environments. G3 **6**:589–597.

Liu, H.-J., Jian, L., Xu, J., Zhang, Q., Zhang, M., Jin, M., Peng, Y., Yan, J., Han, B., Liu, J., et al. (2020b). High-throughput CRISPR/Cas9 mutagenesis streamlines trait gene identification in maize. Plant Cell **32**:1397–1413.

Liu, H.-J., Wang, X., Xiao, Y., Luo, J., Qiao, F., Yang, W., Zhang, R., Meng, Y., Sun, J., Yan, S., et al. (2020a). CUBIC: an atlas of genetic architecture promises directed maize improvement. Genome Biol. **21**:20.

Liu, N., Du, Y., Warburton, M.L., Xiao, Y., and Yan, J. (2021). Phenotypic plasticity contributes to maize adaptation and heterosis. Mol. Biol. Evol. **38**:1262–1275.

Liu, Y., Bai, Y., Li, N., Li, M., Liu, W., Yun, D.J., Liu, B., and Xu, Z.Y. (2022). HEXOKINASE1 forms a nuclear complex with the PRC2 subunits CURLY LEAF and SWINGER to regulate glucose signaling. J. Integr. Plant Biol. **64**:1168–1180.

Lynch, M., and Walsh, B. (1998). Genetics and Analysis of Quantitative Traits, 1st Edition (Sinauer Associates), p. 980p.

Malosetti, M., Ribaut, J.-M., and van Eeuwijk, F.A. (2013). The statistical analysis of multi-environment data: modeling genotype-by-environment interaction and its genetic basis. Front. Physiol. **4**:44.

Mangin, B., Casadebaig, P., Cadic, E., Blanchet, N., Boniface, M.-C., Carrère, S., Gouzy, J., Legrand, L., Mayjonade, B., Pouilly, N., et al. (2017). Genetic control of plasticity of oil yield for combined abiotic stresses using a joint approach of crop modelling and genome-wide association. Plant Cell Environ. **40**:2276–2291.

Matsoukas, I.G., Massiah, A.J., and Thomas, B. (2013). Starch metabolism and antiflorigenic signals modulate the juvenile-to-adult phase transition in Arabidopsis. Plant Cell Environ. **36**:1802–1811.

Meng, X., Muszynski, M.G., and Danilevskaya, O.N. (2011). The FT-like ZCN8 gene functions as a floral activator and is involved in photoperiod sensitivity in maize. Plant Cell **23**:942–960.

Murakami, M., Yamashino, T., and Mizuno, T. (2004). Characterization of circadian-associated APRR3 pseudo-response regulator belonging to the APRR1/TOC1 quintet in Arabidopsis thaliana. Plant Cell Physiol. **45**:645–650.

Nicotra, A.B., Atkin, O.K., Bonser, S.P., Davidson, A.M., Finnegan, E.J., Mathesius, U., Poot, P., Purugganan, M.D., Richards, C.L., Valladares, F., and van Kleunen, M. (2010). Plant phenotypic plasticity in a changing climate. Trends Plant Sci. **15**:684–692.

Pigliucci, M. (2005). Evolution of phenotypic plasticity: where are we going now? Trends Ecol. Evol. **20**:481–486.

Alvarez Prado, S., Sadras, V.O., and Borrás, L. (2014). Independent genetic control of maize (Zea mays L.) kernel weight determination and its phenotypic plasticity. J. Exp. Bot. **65**:4479–4487.

Rauw, W.M., and Gomez-Raya, L. (2015). Genotype by environment interaction and breeding for robustness in livestock. Front. Genet. **6**:310.

Sasaki, E., Zhang, P., Atwell, S., Meng, D., and Nordborg, M. (2015). "Missing" G x E variation controls flowering time in Arabidopsis thaliana. PLoS Genet. **11**:e1005597.

Schneider, H.M., Klein, S.P., Hanlon, M.T., Nord, E.A., Kaeppler, S., Brown, K.M., Warry, A., Bhosale, R., and Lynch, J.P. (2020). Genetic control of root architectural plasticity in maize. J. Exp. Bot. **71**:3185–3197.

Schneider, J.R., Chadee, D.D., Mori, A., Romero-Severson, J., and Severson, D.W. (2011). Heritability and adaptive phenotypic plasticity of adult body size in the mosquito Aedes aegypti with implications for dengue vector competence. Infect. Genet. Evol. **11**:11–16.

Sommer, R.J. (2020). Phenotypic plasticity: from theory and genetics to current and future challenges. Genetics **215**:1–13.

Sultan, S.E. (2000). Phenotypic plasticity for plant development, function and life history. Trends Plant Sci. **5**:537–542.

Tsai, A.Y.-L., and Gazzarrini, S. (2014). Trehalose-6-phosphate and SnRK1 kinases in plant development and signaling: the emerging picture. Front. Plant Sci. **5**:119.

Ungerer, M.C., Halldorsdottir, S.S., Purugganan, M.D., and Mackay, T.F.C. (2003). Genotype-environment interactions at quantitative trait loci affecting inflorescence development in Arabidopsis thaliana. Genetics **165**:353–365.

Vanous, A., Gardner, C., Blanco, M., Martin-Schwarze, A., Wang, J., Li, X., Lipka, A.E., Flint-Garcia, S., Bohn, M., Edwards, J., and Lübberstedt, T. (2019). Stability analysis of kernel quality traits in exotic-derived doubled haploid maize lines. Plant Genome **12**:170114.

Wallace, D.H., Zobel, R.W., and Yourstone, K.S. (1993). A whole-system reconsideration of paradigms about photoperiod and temperature control of crop yield. Theor. Appl. Genet. **86**:17–26.

Weber, S.L., and Scheiner, S.M. (1992). The genetics of phenotypic plasticity. IV. Chromosomal localization. J. Evolution. Biol. **5**:109–120.

Xiao, J., Liu, B., Yao, Y., Guo, Z., Jia, H., Kong, L., Zhang, A., Ma, W., Ni, Z., Xu, S., et al. (2022). Wheat genomic study for genetic improvement of traits in China. Sci. China Life Sci. **65**:1718–1775.

Yang, J., Ferreira, T., Morris, A.P., Medland, S.E., Genetic Investigation of ANthropometric Traits GIANT Consortium, DIAbetes Genetics Replication And Meta-analysis DIAGRAM Consortium, Madden, P.A.F., Heath, A.C., Martin, N.G., Montgomery, G.W., et al. (2012). Conditional and joint multiple-SNP analysis of GWAS summary statistics identifies additional variants influencing complex traits. Nat. Genet. **44**:369–375. S1-S3.

Yang, J., Lee, S.H., Goddard, M.E., and Visscher, P.M. (2011). GCTA: a tool for genome-wide complex trait analysis. Am. J. Hum. Genet. **88**:76–82.

Yano, K., Morinaka, Y., Wang, F., Huang, P., Takehara, S., Hirai, T., Ito, A., Koketsu, E., Kawamura, M., Kotake, K., et al. (2019). GWAS with principal component analysis identifies a gene comprehensively controlling rice architecture. Proc. Natl. Acad. Sci. USA **116**:21262–21267.

Yoshida, S. (1981). Fundamentals of Rice Crop Science (IRRI), p. 269.

Zan, Y., and Carlborg, Ö. (2020a). Dissecting the genetic regulation of yeast growth plasticity in response to environmental changes. Genes **11**:1279.

Zan, Y., and Carlborg, Ö. (2020b). Dynamic genetic architecture of yeast response to environmental perturbation shed light on origin of cryptic genetic variation. PLoS Genet. **16**:e1008801.

Zhou, X., and Stephens, M. (2012). Genome-wide efficient mixed-model analysis for association studies. Nat. Genet. **44**:821–824.